Analysis of resonant population transfer in time-dependent elliptical quantum billiards

Jakob Liss, Benno Liebchen,* and Peter Schmelcher†
Zentrum für Optische Quantentechnologien, Universität Hamburg, Luruper Chaussee 149, 22761 Hamburg, Germany
(Received 11 October 2012; published 22 January 2013)

A Fermi golden rule for population transfer between instantaneous eigenstates of elliptical quantum billiards with oscillating boundaries is derived. Thereby the occurrence of both the recently observed resonant population transfer between instantaneous eigenstates and the empirical criterion stating that these transitions occur when the driving frequency matches the mean difference of the latter [Lenz *et al.*, New J. Phys. **13**, 103019 (2011)] is explained. As a second main result a criterion judging which resonances are resolvable in a corresponding experiment of certain duration is provided. Our analysis is complemented by numerical simulations for three different driving laws. The corresponding resonance spectra are in agreement with the predictions of both criteria.

DOI: 10.1103/PhysRevE.87.012912 PACS number(s): 05.45.Mt, 03.65.Ge

I. INTRODUCTION

Classical driven billiards of varying geometry have been subjected to intensive research over the past several years [1–13]. While billiards are, in general, important models to study aspects of nonlinear dynamics, semiclassics, or (quantum) chaos [14,15], driven billiards additionally facilitate the study of nonequilibrium dynamics. As one of the key topics concerning driven billiards, Fermi acceleration (FA) and the related conditions for its occurrence have gained much attention [5–13]. Fermi acceleration describes the unbounded growth of energy of particles that repeatedly interact with a time-dependent potential that is usually modeled by a moving billiard boundary and was originally proposed by Fermi as a possible mechanism to explain high-energetic cosmic radiation [16]. The infamous Fermi-Ulam model (FUM) is basically a one-dimensional billiard with a moving boundary and it was found that FA is present in the FUM only for nonsmooth driving laws [17]. The general conditions for the occurrence of FA are still under debate. Originally it was assumed that a sufficient condition for the occurrence of FA in a driven two-dimensional billiard is the presence of chaotic regions in the phase space of the corresponding static billiard [13]. However, it turned out that driving an oval-shaped billiard that has a mixed phase space in a certain mode does not lead to FA [18]. In contrast, it was shown that the classical driven elliptical billiard does show FA, although its static counterpart is completely integrable [5,10]. Furthermore, while correlated motion suppresses FA for smooth driving in the FUM, it was found that correlations can even cause exponential FA for smooth driving laws in a related two-dimensional model [11,12].

Although it is known that periodically driven quantum billiards with a discrete Floquet spectrum cannot exhibit FA [19], it is natural to complement the study of the classical dynamics of a system by analyzing its quantum behavior. While one finds many studies to the quantum version of the one-dimensional FUM (see Refs. [20–22], and references therein), literature is very sparse on driven quantum billiards of higher dimensions [23–25].

In particular, Ref. [23] presents a method to solve the time-dependent elliptical quantum billiard. The main result was the numerical observation of resonances in the population transfer probability between instantaneous energy eigenstates. These transitions could be reproduced in an effective Rabi model and captured by a criterion stating that resonances occur whenever the difference of corresponding time-averaged energy eigenvalues matches an integer multiple of the driving frequency. However, an explanation for this criterion was not given in Ref. [23].

Here we develop a systematic perturbative analysis of population transfer for the system analyzed in Ref. [23] and a generalized driving law. In this framework a Fermi golden rule [26] is derived for elliptical quantum billiards with oscillating boundaries that explains the key observations in Ref. [23], i.e., the occurrence of resonant population transfer between instantaneous eigenstates and the empirical criterion relating these resonances with the spectrum of instantaneous eigenstates and the driving frequency. As a second major result we provide a criterion to decide whether a predicted resonance can be resolved in a possible experiment of a certain duration. Finally, the numerical studies in Ref. [23] are complemented by a corresponding analysis of further driving laws. The predictions derived within our perturbative analysis will be shown to provide perfect agreement with the numerical results in all cases.

This work is structured as follows. Section II A provides a short summary of the solution of the time-dependent elliptical quantum billiard as developed in Ref. [23], followed by transformations that bring the Schrödinger equation into a form being convenient for the application of time-dependent perturbation theory. In Sec. II B the transition rate between two instantaneous eigenstates per unit time is calculated in first-order perturbation theory and an approximate population dynamics in the near-resonance case is derived. We find a criterion for the resolvability of predicted resonances in a possible experiment of certain duration. Finally, in Sec. III we present and analyze numerical results for three different periodic driving laws.

II. TIME-DEPENDENT ELLIPTICAL BILLIARD AND ITS ANALYTIC TREATMENT

In the following, we first summarize our approach to a numerical solution of the time-dependent Schrödinger equation of the elliptical billiard as presented in Ref. [23]. We

*benno.liebchen@physnet.uni-hamburg.de
†peter.schmelcher@physnet.uni-hamburg.de

transform the time-dependent Schrödinger equation (TDSE) into a convenient form and finally develop a perturbative approach for the periodically driven billiard in Sec. II B.

A. Setup

A wave function $\Psi(\vec{x},t)$ in a driven elliptical billiard obeying the TDSE

$$i\hbar\partial_t\Psi(\vec{x},t) = -\frac{\hbar^2}{2\mu}\Delta\Psi(\vec{x},t) \tag{1}$$

is subject to Dirichlet boundary conditions $\Psi(\vec{x},t)|_{\partial B} = 0$ on a boundary ∂B of elliptical shape:

$$\partial B = \left\{\vec{x} = (x,y)^\intercal \in \mathbb{R}^2 \,\middle|\, \frac{x^2}{a^2} + \frac{y^2}{b^2} = 1\right\}. \tag{2}$$

Here the semiaxes of the elliptical boundary a and b are assumed to be arbitrary smooth functions of time, i.e., $a = a(t)$ and $b = b(t)$.

The time-dependent boundary conditions can be handled by a coordinate transformation [23]

$$\rho_t : \begin{pmatrix} x \\ y \end{pmatrix} \mapsto \begin{pmatrix} \eta \\ \xi \end{pmatrix} = \begin{pmatrix} \frac{1}{a(t)} & 0 \\ 0 & \frac{1}{b(t)} \end{pmatrix} \begin{pmatrix} x \\ y \end{pmatrix} \tag{3}$$

that maps the time-dependent elliptical boundary onto a static boundary of the shape of a unit circle. Applying Eq. (3) to Eq. (1), together with a unitary transformation

$$U(x,y,t) = \exp\left[-\frac{i\mu}{2\hbar}\left(\frac{\dot{a}(t)x^2}{a(t)} + \frac{\dot{b}(t)y^2}{b(t)}\right)\right], \tag{4}$$

and extracting a volume-dependent prefactor $\sqrt{a(t)b(t)}$ from the wave function $\Psi(\vec{x},t)$, we are led to an effective Schrödinger equation (SE)

$$i\hbar\partial_t\Lambda(\eta,\xi,t) = H^e(\eta,\xi,t)\Lambda(\eta,\xi,t), \tag{5}$$

where the effective Hamiltonian H^e contains time derivatives of the prefactor $\sqrt{a(t)b(t)}$ and of the unitary transformation U of the left-hand side of the TDSE:

$$H^e(\eta,\xi,t) = \frac{-\hbar^2}{2\mu}\left(\frac{1}{a^2(t)}\frac{\partial^2}{\partial\eta^2} + \frac{1}{b^2(t)}\frac{\partial^2}{\partial\xi^2}\right) + \frac{1}{2}\mu[a(t)\ddot{a}(t)\eta^2 + b(t)\ddot{b}(t)\xi^2]. \tag{6}$$

The introduction of the unitary transformation (4) ensures that H^e is Hermitian. Due to the extracted prefactor $\sqrt{a(t)b(t)}$, the effective wave function

$$\Lambda(\eta,\xi,t) := \sqrt{a(t)b(t)}\, U(\rho_t^{-1}(\eta,\xi),t)\Psi(\rho_t^{-1}(\eta,\xi),t) \tag{7}$$

is normalized to 1 on the domain boundary of the unit circle $C := \{\vec{x} = (x,y)^\intercal \in \mathbb{R}^2 | x^2 + y^2 \leqslant 1\}$ and the coordinate transformation (3) makes Λ subject to the Dirichlet boundary condition $\Psi(\vec{x},t)|_{\partial C} = 0$. The reader is referred to Ref. [23] for a similar, more detailed derivation of the effective Hamiltonian and equations of motion.

A complete set of orthonormal functions on C is given by the eigenfunctions of the static circular billiard [27,28]

$$\Phi_{n,m}(\rho,\phi) = \frac{1}{\sqrt{\pi}\, J_{m+1}(k_{m,n})} J_m(k_{m,n}\rho)e^{im\phi}. \tag{8}$$

Here ρ and ϕ can be calculated from η and ξ by $\eta = \rho\cos\phi$ and $\xi = \rho\sin\phi$; J_m is the cylindrical Bessel function of order m and $k_{m,n}$ is its nth root; n and m are called the radial and angular quantum number, respectively, for obvious reasons. If we expand the effective wave function Λ in terms of the eigenfunctions of the static circular billiard, the effective SE (5) becomes a linear homogeneous ordinary differential equation of first order in time and can thus be solved numerically by standard methods [23].

A main result of Ref. [23] was the observation of resonant population transfer between so-called instantaneous eigenstates of

$$H_M = \frac{-\hbar^2}{2\mu}\left(\frac{1}{a^2(t)}\frac{\partial^2}{\partial\eta^2} + \frac{1}{b^2(t)}\frac{\partial^2}{\partial\xi^2}\right). \tag{9}$$

We understand instantaneous eigenstates as follows. The semiaxes a and b are parameters of H_M that change in time. If we evolve our system solely by H_M in the SE, start the system in an initial state that corresponds to an eigenstate of H_M at $t = 0$, and change a and b sufficiently slowly, then we define the instantaneous eigenstate of H_M at time t as the time-evolved wave function of the system at time t in accordance with the adiabatic theorem of quantum mechanics [29].

The Hamiltonian H_M (9) is part of the effective Hamiltonian H^e [Eq. (6)]. Its complementary part is

$$H_F = H^e - H_M = \tfrac{1}{2}\mu[a(t)\ddot{a}(t)\eta^2 + b(t)\ddot{b}(t)\xi^2]. \tag{10}$$

Population transfer between instantaneous eigenstates of H_M takes place by two different mechanisms in the billiard. First, as a and b are of course not changed sufficiently slowly, diabatic population transfer between the instantaneous eigenstates of H_M will take place. Additionally, the Hamiltonian H_F triggers population transfer as it is nondiagonal in the basis set of instantaneous eigenstates of H_M.

Introducing the volume of the elliptical billiard $V(t) = a(t)b(t)$ and the ratio of the semiaxes $r(t) = b(t)/a(t)$, H_M can be rewritten in the much more convenient form

$$H_M = \frac{\hbar^2}{\mu V(t)} M[r(t)], \tag{11}$$

where we call

$$M(r) := -\frac{1}{2}\left(r\frac{\partial^2}{\partial\eta^2} + \frac{1}{r}\frac{\partial^2}{\partial\xi^2}\right) \tag{12}$$

the Mathieu operator as its eigenfunctions are just ordinary and modified Mathieu functions as they appear in the solutions of the static elliptical billiard. If we label the eigenstates of $M(r)$ as $|n;r\rangle$ with eigenvalue $q_n(r)$, $|n;r(t)\rangle$ are of course the instantaneous eigenstates of H_M and $E_n(t) = \frac{\hbar^2}{\mu V(t)}q_n[r(t)]$ are the corresponding instantaneous eigenvalues of H_M, i.e., we have

$$H_M = \sum_{n=1}^{\infty} |n;r(t)\rangle \frac{\hbar^2 q_n[r(t)]}{\mu V(t)} \langle n;r(t)|\,. \tag{13}$$

Note that $M(r)$ is invariant upon the sign change of η and ξ. One can therefore choose its eigenstates $|n;r\rangle$ such that they are also eigenstates of the parity operators that change the sign of η or ξ. In this context, we will refer to $|n;r\rangle$ as having even

or odd η and ξ parity. Note that the effective Hamiltonian H^e [Eq. (6)] is also invariant upon the sign change of η and ξ and consequently couples only instantaneous eigenstates that have the same η and ξ parity. The Hilbert space therefore splits into four uncoupled Hilbert subspaces.

We choose the following ansatz for the effective wave function Λ:

$$|\Lambda(t)\rangle = \sum_n c_n(t) e^{-(i/\hbar)\phi_n(t)} |n;r(t)\rangle \ , \tag{14}$$

with time-dependent expansion coefficients $c_n(t)$ and

$$\phi_n(t) := \int_0^t dt' E_n(t') = \int_0^t dt' \frac{\hbar^2}{\mu V(t')} q_n[r(t')] \tag{15}$$

being the time-integrated instantaneous eigenvalues of H_M. If we put this ansatz into the the SE (5) and note that $\partial_t |n;r(t)\rangle = \dot{r}(\partial_r |n;r\rangle)|_{r=r(t)} \equiv \dot{r}\partial_r |n;r(t)\rangle$, we get a SE for the coefficients $c_n(t)$:

$$\begin{aligned} i\hbar\partial_t c_n(t) = \sum_m c_m(t) e^{-(i/\hbar)[\phi_m(t)-\phi_n(t)]} [\langle n;r(t)|H_F(t)|m;r(t)\rangle \\ - i\hbar\dot{r}(t)\langle n;r(t)|\partial_r|m;r(t)\rangle]. \end{aligned} \tag{16}$$

For nondegenerate eigenstates $|n;r\rangle$ and $|m;r\rangle$, one can express the second matrix element on the right-hand side of Eq. (16) as

$$\langle n;r|\partial_r|m;r\rangle = \begin{cases} \frac{\langle n;r|[\partial_r M(r)]|m;r\rangle}{q_m(r)-q_n(r)} & \text{for} \quad n \neq m \\ \langle n;r|\partial_r|n;r\rangle & \text{for} \quad n = m. \end{cases} \tag{17}$$

It is now interesting to notice that the representation of $M(r)$ in the eigenbasis of the static circular billiard (8) $\langle \Phi_{n',m'}|M(r)|\Phi_{n,m}\rangle$ not only is a Hermitian but a real symmetric matrix [cf. Eq. (A14) in the Appendix). We can therefore choose the expansion coefficients of the eigenstates of $M(r)$ in the eigenbasis of the static circular billiard, $\langle \Phi_{n',m'}|n;r\rangle$, to be real. It follows that also the expansion coefficients of $\partial_r |n;r\rangle$, $\langle \Phi_{n',m'}|\partial_r|n;r\rangle$, are real. Thus

$$\langle n;r|\partial_r|n;r\rangle = \sum_{n',m'} \langle n;r|\Phi_{n',m'}\rangle \langle \Phi_{n',m'}|\partial_r|n;r\rangle \tag{18}$$

is also real. In contrast, due to normalization of the eigenstates $|n;r\rangle$, expression (18) has to be purely imaginary and is therefore identical zero. Noting that

$$\begin{aligned} \partial_r M(r) &= \frac{\partial^2}{\partial\eta^2} - \frac{1}{r^2}\frac{\partial^2}{\partial\xi^2} = \frac{1}{r}\left(r\frac{\partial^2}{\partial\eta^2} - \frac{1}{r}\frac{\partial^2}{\partial\xi^2}\right) \\ &= \frac{M(ir)}{ir} \end{aligned} \tag{19}$$

further simplifies Eq. (17). From now on we will restrict ourselves to periodic driving laws, i.e., $a(t+\frac{2\pi}{\omega}) = a(t)$ and $b(t+\frac{2\pi}{\omega}) = b(t)$, and restrict our analytical treatment to cases where all populated instantaneous eigenstates are nondegenerate. Unpopulated energy levels may of course still exhibit crossings. Note that the restriction to periodic driving laws and nondegenerate eigenstates also includes all cases that are discussed in Ref. [23] and is not as restrictive as it might seem at first: The following analysis will show that one can control very precisely which eigenstates will get populated upon driving by choosing suitable driving parameters. Also, the occurrence of crossings itself is solely determined by the parameter r [compare Eqs. (11)–(13)] and can thus be controlled: To make sure that populated eigenstates do not become degenerate upon driving one just has to choose the driving such that no values of r are assumed that make two of these eigenstates degenerate. Correspondingly, the occurrence of crossings in the spectrum of instantaneous eigenstates can be controlled via the driving amplitude, the initial eccentricity of the ellipse, and of course the driving mode. In contrast to the analytical treatment, our numerical simulations work equally well for cases of populated degenerate eigenstates and have been checked for convergence in all cases.

We introduce a rescaled dimensionless time $\tau := \frac{\omega}{2\pi}t$ and finally put Eqs. (17) and (19) back into Eq. (16):

$$\begin{aligned} i\partial_\tau c_n(\tau) = \sum_m c_m(\tau) e^{-(2\pi i/\hbar\omega)[\phi_m(\tau)-\phi_n(\tau)]} \\ \times \frac{\omega}{2\pi\hbar}\langle n;r(\tau)|H_F(\tau)|m;r(\tau)\rangle \\ + \sum_{m\neq n} c_m(\tau) e^{-(2\pi i/\hbar\omega)[\phi_m(\tau)-\phi_n(\tau)]} \\ \times \frac{\dot{r}(\tau)}{r(\tau)}\frac{\langle n;r(\tau)|M[ir(\tau)]|m;r(\tau)\rangle}{q_n[r(\tau)]-q_m[r(\tau)]}. \end{aligned} \tag{20}$$

We point out that the modulus of the first term in Eq. (20) depends linearly on the driving frequency ω while the modulus of the second term is independent of ω. We therefore expect the first term to be dominant for large driving frequencies, while the second one should be dominant for small driving frequencies and should especially couple neighboring instantaneous eigenstates due to the denominator $q_n[r(\tau)] - q_m[r(\tau)]$.

Obviously, due to periodic driving, all terms on the right-hand side of Eq. (20) but the coefficients $c_m(\tau)$ and the phase factors $\exp\{-2\pi i[\phi_m(\tau) - \phi_n(\tau)]/\hbar\omega\}$ are one-period functions in τ. It is therefore possible to represent them by discrete Fourier transforms. Before we do so, we split $\phi_m(\tau) - \phi_n(\tau)$ into a nonperiodic part $\hbar\nu_{mn}\tau := [\phi_m(1) - \phi_n(1)]\tau$ and a one-periodic part $\hbar\Delta\nu_{mn}(\tau)$:

$$\phi_m(\tau) - \phi_n(\tau) = \hbar\nu_{mn}\tau + \hbar\Delta\nu_{mn}(\tau). \tag{21}$$

We then combine the one-periodic phase factor $\exp[-2\pi i\Delta\nu_{mn}(\tau)/\omega]$ with the other one-periodic terms on the right-hand side of Eq. (20) and Fourier transform the results:

$$\begin{aligned} \omega \sum_{l=-\infty}^{l=\infty} F_l^{nm} e^{-2\pi i l\tau} \\ = e^{-(2\pi i/\omega)\Delta\nu_{mn}(\tau)} \frac{\omega}{2\pi\hbar}\langle n;r(\tau)|H_F(\tau)|m;r(\tau)\rangle \ , \end{aligned} \tag{22}$$

$$\begin{aligned} \sum_{l=-\infty}^{l=\infty} D_l^{nm} e^{-2\pi i l\tau} \\ = \begin{cases} e^{-(2\pi i/\omega)\Delta\nu_{mn}(\tau)}\frac{\dot{r}(\tau)}{r(\tau)}\frac{\langle n;r(\tau)\,|\,M[ir(\tau)]\,|\,m;r(\tau)\rangle}{q_n(r(\tau))-q_m[r(\tau)]} & \text{for } n \neq m \\ 0 & \text{for } n = m. \end{cases} \end{aligned} \tag{23}$$

Before we put Eqs. (22) and (23) back into the SE (20), it is useful to perform a unitary transformation $c_n(\tau) = \exp(-i\omega F_0^{nn}\tau)b_n(\tau)$. Note that we do not include D_0^{nn} in

the unitary transformation as it is zero by definition (23) and that F_0^{nn} is completely independent of ω. This unitary transformation, together with Eqs. (22) and (23), leads via Eq. (20) to a SE for the coefficients b_n:

$$i\dot{b}_n(\tau) = \sum_{\substack{m,l \\ m \neq n \text{for} l=0}} e^{2\pi i \theta_l^{nm}\tau}\left(\omega F_l^{nm} + D_l^{nm}\right) b_m(\tau), \quad (24)$$

where we have defined the abbreviation

$$\theta_l^{nm} := \frac{\nu_{nm}}{\omega} + \frac{\omega}{2\pi}\left(F_0^{nn} - F_0^{mm}\right) - l. \quad (25)$$

Note that the solution of Eq. (24) determines the complete physics of periodically driven elliptical quantum billiards.

B. Perturbative analysis

We will now use time-dependent perturbation theory (TDPT) to find an approximate solution of Eq. (24) in first order. To do so, we formally affix a parameter λ to F_l^{nm} and D_l^{nm} to keep track of the order of perturbation and will set λ to 1 at the end of our calculation: $F_l^{nm} = \lambda F_l^{nm}$ and $D_l^{nm} = \lambda D_l^{nm}$. An expansion of $b_n(\tau)$ in λ gives $b_n(\tau) = \sum_{p=0}^{\infty} \lambda^p b_n^{(p)}(\tau)$. As λ should track the order of perturbation, it is natural to choose the initial values of $b_n^{(p)}$ as $b_n^{(p)}(0) = \delta_{p,0} b_n(0)$. Inserting this ansatz into Eq. (24) and equating equal powers of λ yields up to first order

$$i\dot{b}_n^{(0)} = 0 \Rightarrow b_n^{(0)} = \text{const} = b_n(0), \quad (26)$$

$$i\dot{b}_n^{(1)} = \sum_{\substack{m,l \\ m \neq n \text{for} l=0}} e^{2\pi i \theta_l^{nm}\tau}\left(\omega F_l^{nm} + D_l^{nm}\right) b_m(0) \quad (27)$$

$$\Rightarrow b_n^{(1)}(\tau) = \sum_{\substack{m,l \\ m \neq n \text{for} l=0}} \frac{e^{2\pi i \theta_l^{nm}\tau} - 1}{2\pi i \theta_l^{nm}} \times \left(\omega F_l^{nm} + D_l^{nm}\right) b_m(0). \quad (28)$$

1. Population transfer probability

We are now able to calculate the population transfer probability between two instantaneous eigenstates that will lead to a systematic understanding of resonant population transfer as it was observed in Ref. [23]. For this purpose we assume that the wave function $|\Lambda\rangle$ was initially in the (undriven) eigenstate $|k;r\rangle$ and then calculate the evolution of the population of the eigenstate $|n;r\rangle$ $(n \neq k)$. Population transfer in first order gives

$$p_{nk}^1(\tau) := \left|b_n^{(1)}(\tau)\right|^2 = \sum_{l,l'} \frac{e^{2\pi i \theta_l^{nk}\tau} - 1}{2\pi\theta_l^{nk}} \frac{e^{-2\pi i \theta_{l'}^{nk}\tau} - 1}{2\pi\theta_{l'}^{nk}} \times \left(\omega F_l^{nk} + D_l^{nk}\right)\left(\omega F_{l'}^{*nk} + D_{l'}^{*nk}\right). \quad (29)$$

We would like to calculate a population transition rate per unit time from Eq. (29), which is defined as $\Gamma_{nk}^1 := \lim_{\tau\to\infty} p_{nk}^1(\tau)/\tau$. Note that $(e^{2\pi i\theta_l^{nk}\tau} - 1)/2\pi\theta_l^{nk} = ie^{\pi i\theta_l^{nk}\tau}\sin(\pi\theta_l^{nk}\tau)/\pi\theta_l^{nk}$ grows linearly with τ for $\theta_l^{nk} = 0$ while it oscillates periodically with an amplitude $1/\pi\theta_l^{nk}$ (which is independent of τ) for $\theta_l^{nk} \neq 0$. Due to $\theta_l^{nk} - \theta_{l'}^{nk} = l' - l$, we can therefore neglect all terms in Eq. (29) with $l \neq l'$ for τ being sufficiently large

$$\Gamma_1^{nk} := \lim_{\tau\to\infty} \frac{p_{nk}^1(\tau)}{\tau} = \lim_{\tau\to\infty} \sum_l \frac{\sin^2\pi\theta_l^{nk}\tau}{\tau\left(\pi\theta_l^{nk}\right)^2} \left|\omega F_l^{nk} + D_l^{nk}\right|^2 = \sum_l \delta\left(\theta_l^{nk}\right)\left|\omega F_l^{nk} + D_l^{nk}\right|^2. \quad (30)$$

By applying appropriate transformations, we have handled the time-dependent boundary conditions of the billiard by introduction of a time-dependent external potential. This enabled us to derive Eq. (30), which is a Fermi golden rule [26] for driven elliptical quantum billiards. It states that efficient population transfer in first order between the instantaneous eigenstates $|k;r\rangle$ and $|n;r\rangle$ is only possible for $\theta_l^{nk} = 0$. We can now use Eq. (25) to calculate corresponding resonance frequencies

$$\omega_{\text{res}}^{nk,l} = \frac{l \pm \sqrt{l^2 - 4\nu_{nk}\delta F_0^{nk}}}{2\delta F_0^{nk}}, \quad (31)$$

where $2\pi \cdot \delta F_0^{nk} := F_0^{nn} - F_0^{kk}$ has been defined. Numerical experience shows that δF_0^{nk} is usually a very small quantity. The "+" term in Eq. (31) thus corresponds to a very large resonance frequency. Restricting ourselves to not too strongly driven billiards, we will neglect this term from now on. If we develop the "−" term in Eq. (31) about $\delta F_0^{nk} \approx 0$ and use the definition of ν_{nk} in Eq. (21) above, we find

$$l\omega_{\text{res}}^{nk,l} = \nu_{nk} = \int_0^1 E_n(\tau') - E_k(\tau')d\tau'. \quad (32)$$

Thus, only when the one-period average difference of two instantaneous energy eigenvalues matches an integer multiple of the driving frequency can resonant population transfer between the corresponding instantaneous eigenstates occur. This is precisely the empirically found criterion in Ref. [23] and has herewith a theoretical basis. The result justifies to call the Fourier summation index l "photon process order" of a population transfer in analogy to the interaction of light and matter.

2. Applicability of first-order TDPT

Not all predicted resonance frequencies (31) are of equal importance with respect to their experimental observation and we will now derive a criterion to discriminate them. In the resonant case $\theta_l^{nk} = \theta_{l'}^{nk} = 0$, Eq. (29) reduces to

$$p_{nk}^1 = \tau^2 \sum_l \left|\omega F_l^{nk} + D_l^{nk}\right|^2. \quad (33)$$

The reader is reminded that Eq. (33) only holds for $n \neq k$, while for $n = k$, $p_{kk}^1 = 0$ holds as $\theta_l^{kk} = 0$ implies $l = 0$ and this case just had been excluded from the summation in Eq. (28). Consequently, the instantaneous eigenstate $|k;r\rangle$ gets exclusively depopulated in first-order TDPT. We can therefore calculate the time τ_{int} at which the population p_k of

the instantaneous eigenstate $|k;r\rangle$ gets negative and therefore unphysical:

$$p_k(\tau_{\text{int}}) = 1 - \sum_{\theta_l^{nk}\equiv 0} p_{nk}^1(\tau_{\text{int}}) \stackrel{!}{=} 0 \tag{34}$$

$$\Rightarrow \tau_{\text{int}} = \frac{1}{\sqrt{\sum_{\theta_l^{nk}\equiv 0}\left|\omega F_l^{nk} + D_l^{nk}\right|^2}}. \tag{35}$$

The summation index $\theta_l^{nk} \equiv 0$ in Eqs. (34) and (35) means that it should only be summed over states n and photon process orders l that satisfy the resonance condition $\theta_l^{nk} \equiv 0$. This means in all practical examples that the sum only consists of a single term.

The term τ_{int} is a measure of how fast a population probability transfer takes place. It is thus reasonable that we will not be able to fully resolve resonances that correspond to an interaction time τ_{int} that is much larger than the actual run-time τ_{run} of a possible experiment. In this case, population transfer will have been stopped before the maximal theoretically possible amount of population probability will have been transferred from one instantaneous eigenstate to the other and our ability to resolve a resonance in corresponding observations is diminished.

In contrast, we understand that the transition rate (30) has been calculated in the limit $\tau \to \infty$ and the included δ function is the result of a convergence process. In order to have the system meet the predictions of first-order TDPT, τ_{int} should be large enough such that a delta function $\delta(\theta)$ is a good approximation of $\sin^2 \pi\theta\tau/\tau(\pi\theta)^2$ as it appears in the derivation of Eq. (30). Obviously, such a criterion depends on the density of the θ_l^{nk} about $\theta = 0$. We therefore define a lower threshold

$$\tau_{\text{low}} := \max_{|\theta_l^{nk}|\neq 0} \frac{1}{\left|\theta_l^{nk}\right|}, \tag{36}$$

where only θ_l^{nk} should be considered in Eq. (36), whose corresponding resonant probability transitions (i.e., for the case $\theta_l^{nk} = 0$) have interaction times of the order of magnitude of τ_{run} such that they are relevant for the experiment. In summary, we expect predicted resonances to be fully resolved if

$$\tau_{\text{low}} \ll \tau_{\text{int}} < \tau_{\text{run}} \tag{37}$$

holds. The discussion of concrete driving laws in Sec. III shows that this criterion is in excellent agreement with our numerical simulations.

3. Rotating wave approximation

Interestingly, Eq. (37) justifies a rotating wave approximation in Eq. (24) [30]. This allows us to calculate approximate population dynamics of the system that, in contrast to Eq. (29), conserve the total population probability.

For simplicity, we will assume that there is only one θ_l^{nk} close to zero. A rotating wave approximation simply sets all other terms in Eq. (24) that do not contain this θ_l^{nk} to zero as they are comparatively fast oscillating; thus we are left with with an effective two-level system

$$\begin{aligned} i\dot{b}_n(\tau) &= e^{2\pi i\theta_l^{nk}\tau}\left(\omega F_l^{nk} + D_l^{nk}\right)b_k(\tau), \\ i\dot{b}_k(\tau) &= e^{-2\pi i\theta_l^{nk}\tau}\left(\omega F_l^{kn} + D_l^{kn}\right)b_n(\tau). \end{aligned} \tag{38}$$

The behavior of such a system is very well understood. A discussion in terms of Bloch equations is for instance given in Ref. [31]. Equations (38) in particular explain why the population dynamics in Ref. [23] are reminiscent of Rabi oscillations. The effective Rabi frequency Ω_{eff} can be calculated (see, e.g., Ref. [31]) to be

$$\begin{aligned} \Omega_{\text{eff}} &= \sqrt{\left(2\pi\theta_l^{nk}\right)^2 + 4\left|\omega F_l^{nk} + D_l^{nk}\right|^2} \\ &= \sqrt{\left(2\pi\theta_l^{nk}\right)^2 + 4\frac{1}{\tau_{\text{int}}^2}}, \end{aligned} \tag{39}$$

which yields a beating period T_B of the population dynamics

$$T_B := \frac{2\pi}{\Omega_{\text{eff}}} = \frac{\pi\tau_{\text{int}}}{\sqrt{1 + \left(\pi\theta_l^{nk}\tau_{\text{int}}\right)^2}}. \tag{40}$$

In summary, if we assume the system to have initially been in state k, the population dynamics of state n is given by

$$p_n(\tau) = \frac{\sin^2\left(\frac{\pi\tau}{T_B}\right)}{1 + \left(\pi\theta_l^{nk}\tau_{\text{int}}\right)^2}. \tag{41}$$

III. NUMERICAL RESULTS AND DISCUSSION

In this section we will present full numerical simulations of driven elliptical billiards and analyze the results with the developed perturbation theory of Sec. II B. Details of the numerical calculation of the predicted quantities can be found in the Appendix. All numerical calculations have been run for $\tau_{\text{run}} = 100$ periods of driving and $\hbar$ and μ have, without loss of generality, been set to 1. We will always drive the semiaxis $a(t)$ harmonically, i.e.,

$$a(t) = a_0 + A\sin(\omega t), \tag{42}$$

and adjust $b(t)$ such that the billiard is driven in different ways, as will be specified later. To be able to compare the different driving laws, we have chosen to keep the following parameters fixed:

$$a_0 := a(t=0) = 1, \quad A = 0.1, \quad b_0 := b(t=0) = \sqrt{0.51}. \tag{43}$$

These parameters are the same as in Ref. [23].

The energy $E(\tau)$ will be a key observable for the analysis of the billiard dynamics. It is calculated from the expectation value of the Hamiltonian $H = -\frac{\hbar^2}{2\mu}\Delta$ as it appears in Eq. (1):

$$E(\tau) = \langle\Psi(\tau)|-\frac{\hbar^2}{2\mu}\Delta|\Psi(\tau)\rangle. \tag{44}$$

If we apply again the coordinate transformation (3) and the unitary transformation U [Eq. (4)], the energy reads

$$E(\tau) = \langle\Lambda(\tau)|U^\dagger(\tau)H_M(\tau)U(\tau)|\Lambda(\tau)\rangle, \tag{45}$$

where $H_M(\tau)$ is given by Eq. (9). We can therefore calculate $E(\tau)$ by determining the population $p_n(\tau)$ of the eigenstates

of $U^\dagger(\tau)H_M(\tau)U(\tau)$ in $|\Lambda(\tau)\rangle$, weighting these populations with the respective eigenvalues $E_n(\tau)$ of $U^\dagger(\tau)H_M(\tau)U(\tau)$, and sum the results:

$$E(\tau) = \sum_n E_n(\tau)p_n(\tau). \tag{46}$$

Note that, due to U being a unitary transformation, the energy eigenvalues $E_n(\tau)$ of $U^\dagger(\tau)H_M(\tau)U(\tau)$ are actually identical to the instantaneous eigenvalues $E_n(\tau)$ of $H_M(\tau)$.

From now on we refer to the instantaneous eigenstates of $U^\dagger(\tau)H_M(\tau)U(\tau)$ as energy eigenstates. We understand in particular that the instantaneous eigenstates $|n;r(\tau)\rangle$ of $H_M(\tau)$ are in general not identical to the energy eigenstates, but unitarily transformed energy eigenstates, given by $U^\dagger|n;r(\tau)\rangle$. Note that U is also invariant upon the sign change of η and ξ such that an instantaneous eigenstate $|n;r(\tau)\rangle$ and its corresponding energy eigenstate $U^\dagger|n;r(\tau)\rangle$ have the same η and ξ parity.

We will initialize the system in the fourth energy eigenstate (at $\tau = 0$) and calculate the populations $p_n(\tau)$ upon driving. Note that in Ref. [23] instantaneous eigenstates $|n;r(\tau)\rangle$ were used as initial states and for population analyses.

Interestingly, we find that the overlap $|\langle n;r(\tau)|U(\tau)|n;r(\tau)\rangle|^2$ of all relevant instantaneous eigenstates $|n;r(\tau)\rangle$ with their respective energy eigenstates is greater than 94.5% for the parameter regimes analyzed later in Sec. III. We thus expect that the energy eigenstates are similar to the instantaneous eigenstates and also show similar population dynamics. Consequently, we will from now on disregard the differences between $|n;r(\tau)\rangle$ and the energy eigenstates $U^\dagger|n;r(\tau)\rangle$ when analyzing the billiard dynamics perturbatively and will subsequently refer to $|n;r(\tau)\rangle$ simply as energy eigenstates. This approximation enables us to predict the seemingly complicated population dynamics of the energy eigenstates by our perturbation theory for instantaneous eigenstates. Although the population dynamics of the energy eigenstates are not expected to be qualitatively different, some predictions may be compromised quantitatively. For instance, due to the different actions of $U^\dagger(\tau)$ on different $|n;r(\tau)\rangle$, shifts of the resonance frequencies (31) are to be expected. However, as U [Eq. (4)] approaches unity for vanishing ω, these shifts will rather be observed for larger resonance frequencies. We will also find that the resonance shifts become more negligible for higher-order photon processes.

In the approximation of instantaneous eigenstates $|n;r(\tau)\rangle$ being energy eigenstates, a transition to a higher excited state increases the energy $E(\tau)$ [Eq. (46)] while a transition to a lower excited state decreases it. We can therefore determine if a population transition occurs at a certain driving frequency ω upon simulation time τ_{run} by calculating the maximal and minimal energies of the billiard as a function of ω.

A. Axis-ratio-preserving driving law

In the following, we provide numerical solutions for various driving laws and analyze them with the developed perturbation theory of Sec. II B. A simple but illustrative driving law is the so-called axis-ratio-preserving driving law, which merely rescales the billiard by varying its volume $V(\tau)$ while keeping the ratio of the semiaxes $r(\tau)$ constant for all times upon driving. As $a(t)$ is given by Eq. (42), we find $b(t) = r_0 a(t)$ and choose $r_0 = \sqrt{0.51}$ to satisfy Eq. (43).

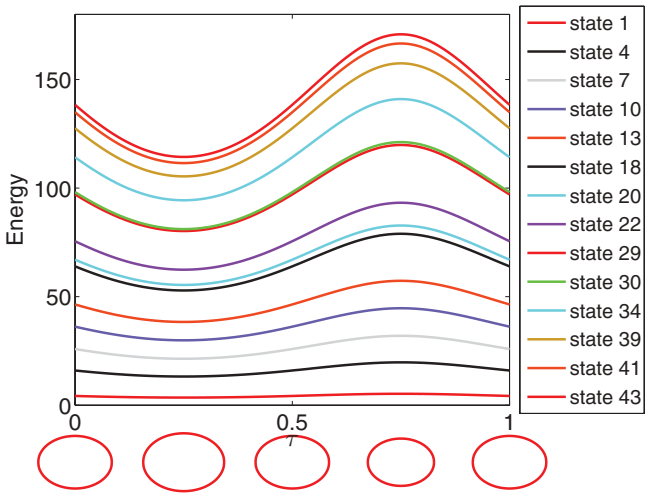

FIG. 1. (Color online) Energy eigenvalues $E_n(\tau)$ of eigenstates $|n;r(\tau)\rangle$ with even η- and ξ-parity eigenvalues for the axis-ratio-preserving driving law. The instantaneous shape of the ellipse at five different values of τ is drawn below the energy eigenvalue curves. The parameters are $a_0 = 1$, $b_0 = \sqrt{0.51}$, and $A = 0.1$.

The axis-ratio-preserving driving law has the nice property that the instantaneous eigenstates $|n;r(\tau)\rangle$ become time independent due to fixed $r(\tau) = r_0$, while the eigenvalues $E_n(\tau)$ stay time dependent, as can be seen from Eq. (13). Their variation is solely given by the global prefactor $1/V(\tau)$, which particularly prevents crossings of energy eigenvalues. Figure 1 shows a sample of eigenvalue curves for one period of driving. The fourth energy eigenstate has even η and ξ parity. Thus, only energy eigenstates in the corresponding sub-Hilbert space couple to the chosen initial state.

In Fig. 2 the dependence of the maximal and minimal energies that has been reached upon driving as a solution of the TDSE in Eq. (1) is plotted depending on the driving frequency ω. We clearly see sharp peaks and dips at certain driving frequencies. The vertical lines represent our predictions of resonance frequencies according to Eq. (31). Note that the observed resonances deviate slightly from the predicted ones, especially for larger driving frequencies. This is due to the unitary transformation U [Eq. (4)] that has been neglected in our considerations, i.e., we apply perturbation theory only to the instantaneous eigenstate $|n;r(\tau)\rangle$ that is most populated in the energy eigenstate $U^\dagger(\tau)|n;r(\tau)\rangle$. Besides this anticipated small deviation, we find very good agreement of the numerical calculations with our predictions. All resonances with a comparatively small interaction time τ_{int} have been resolved, while resonances with very large interaction times could not be observed. Naturally, for interaction times that are longer than (half) the run-time of an experiment τ_{run}, a full population transition from the initial state to some other energy eigenstate cannot happen according to Eq. (41). This is the reason why some peaks in Fig. 2 that correspond to transitions to the same energy eigenstate possess different heights. It is interesting to note that, although the run-time τ_{run} of our numerical simulations was only 100 periods of driving, resonances that correspond to an interaction time of up to 2000 periods of

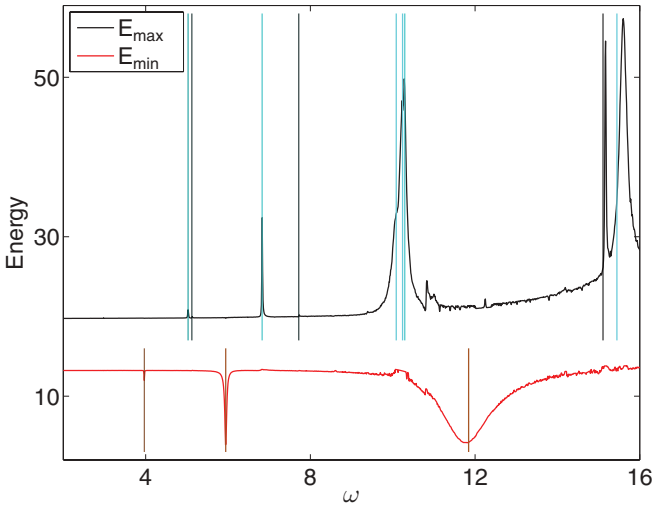

FIG. 2. (Color online) Dependence of the maximal and minimal energies on the driving frequency ω for the axis-ratio-preserving driving law. The vertical lines show all predicted resonance frequencies (31) with an interaction time τ_{int} of less than 2000. The darker the lines are, the longer the corresponding interaction time is. Numerical values can be taken from Table I. The parameters are the same as in Fig. 1.

driving could still be partly resolved in Fig. 2. Table I provides numerical values for all predicted resonance frequencies between 0 and 16 that have an interaction time of less than 2000. It also shows that the lower threshold τ_{low} is always much smaller than the corresponding interaction time τ_{int} such that the first part of Eq. (37) is fulfilled and TDPT of first order is applicable.

One might wonder about a structure of several small peaks, especially for frequencies $\omega \gtrsim 10.5$. We assume that these smaller, not predicted peaks correspond to transitions of second order where population is first transferred to one excited state and then from this state again transferred to yet another energy eigenstate. This is supported, for instance, by a population analysis in Fig. 3 for the small peak at $\omega = 10.81$. We see that the mean (or envelope behavior)

TABLE I. Numerical values for all predicted resonance frequencies between the values 0 and 16 with an interaction time τ_{int} less than 2000. Information is provided on the corresponding lower threshold τ_{low}, the quantum number of the coupling instantaneous eigenstate n, and the photon process order l of the resonance.

$\omega_{\text{res}}^{n4,l}$	τ_{int}	τ_{low}	State n	Order l
3.966	304	0.181	1	3
5.030	328	0.482	7	2
5.122	1014	0.493	10	4
5.944	39.4	0.271	1	2
6.829	133	0.657	10	3
7.720	1098	0.743	13	4
10.09	40.5	0.970	7	1
10.24	17.3	0.985	10	2
10.29	144	0.990	13	3
11.84	4.91	0.540	1	1
15.11	1647	1.77	22	4
15.44	18.7	1.48	13	2

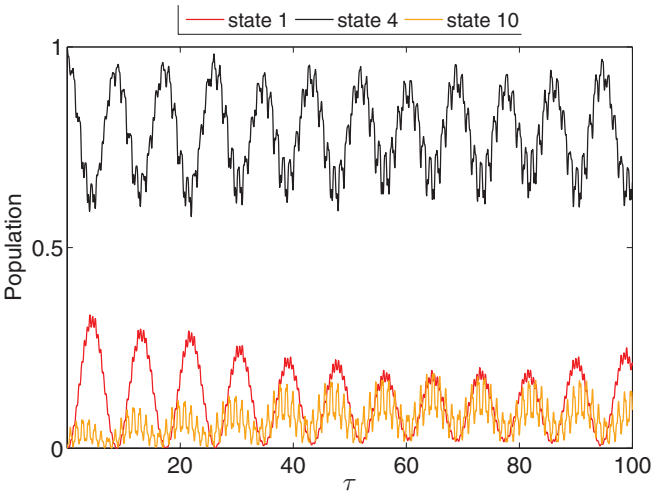

FIG. 3. (Color online) Population dynamics $p_n(\tau)$ for the axis-ratio-preserving driving law at $\omega = 10.81$. The parameters are the same as in Fig. 1.

population of the energetic ground state decreases while the population amplitude of the tenth energy eigenstate increases. This may be interpreted as an interaction of these two states that consecutively leads to a transfer of population that was initially transferred to the ground state and is then pushed to the tenth energy eigenstate. Such a process is not included in the time-dependent perturbation theory of first order in Sec. II B and the dynamics visualized in Fig. 3 are a precursor to the breakdown of this simple theory for higher driving frequencies where indirect transitions become more and more important.

It is also interesting that the resonance at $\omega \approx 15.17$ that corresponds to a four-photon transition from the initial state to the 22nd energy eigenstate is so well resolved, although the interaction time of this resonance is much larger than the interaction time of several resonances that are much worse resolved (see Fig. 4). The reason for this is that the 22nd energy eigenstate has a much higher energy eigenvalue than, for instance, the seventh energy eigenstate. Thus the energy is

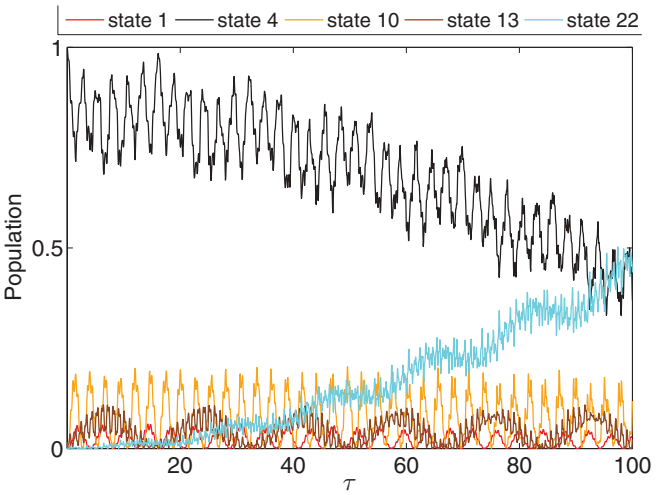

FIG. 4. (Color online) Population dynamics $p_n(\tau)$ for the axis-ratio-preserving driving law at $\omega = 15.17$. The parameters are the same as in Fig. 1.

TABLE II. Analog to Table I, but for the breathing driving law.

$\omega_{\mathrm{res}}^{n4,l}$	τ_{int}	τ_{low}	State n	Order l
2.584	589	0.254	7	4
3.446	150	0.339	7	3
3.972	309	0.178	1	3
5.128	1207	0.504	10	4
5.170	40.0	0.508	7	2
5.954	39.9	0.268	1	2
6.836	151	0.672	10	3
7.807	361	0.728	13	4
10.25	18.8	1.01	10	2
10.35	11.0	1.02	7	1
10.41	63.7	0.970	13	3
11.86	4.90	0.534	1	1
13.18	1284	3.29	20	4
15.21	1019	1.87	22	4
15.62	11.2	1.44	13	2

significantly increased for already a small amount of transferred population probability from the initial state to the 22nd energy eigenstate. As can be seen in Fig. 4, the population of the 22nd energy eigenstate is still less than 0.5 after 100 periods of driving, in agreement with our estimate of the interaction time.

B. Other driving laws

We have seen in the preceding section that the predictions of TDPT work very well for the axis-ratio-preserving driving law. To illustrate the general applicability of the perturbation theory of Sec. II B under the given assumptions, we will analyze two further driving laws. The so-called breathing driving law $b(t) = a(t) - a_0 + b_0$, where $a(t)$ is again given by Eq. (42), was already discussed in Ref. [23]. Figure 5 shows the eigenvalues of energy eigenstates with even η and ξ parity for one period of driving. We see that crossings of energy eigenvalues are, in contrast to Fig. 1, now possible as $r(t)$ is no longer kept constant. The eigenvalues of the

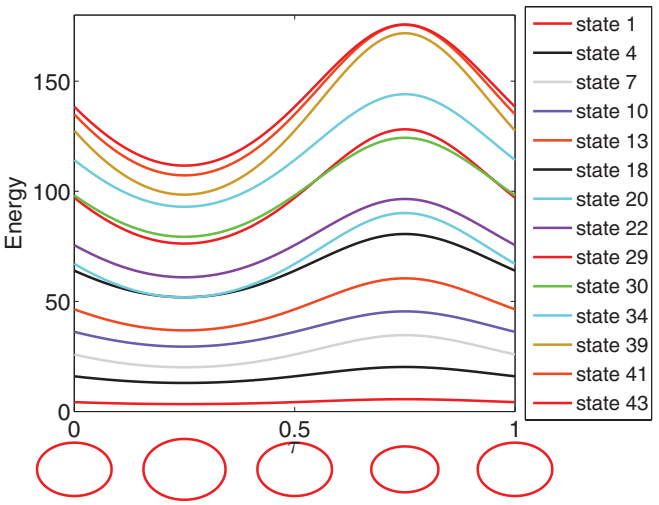

FIG. 5. (Color online) Energy eigenvalues $E_n(\tau)$ of eigenstates $|n;r(\tau)\rangle$ with even η and ξ parity for the breathing driving law. The parameters are the same as in Fig. 1.

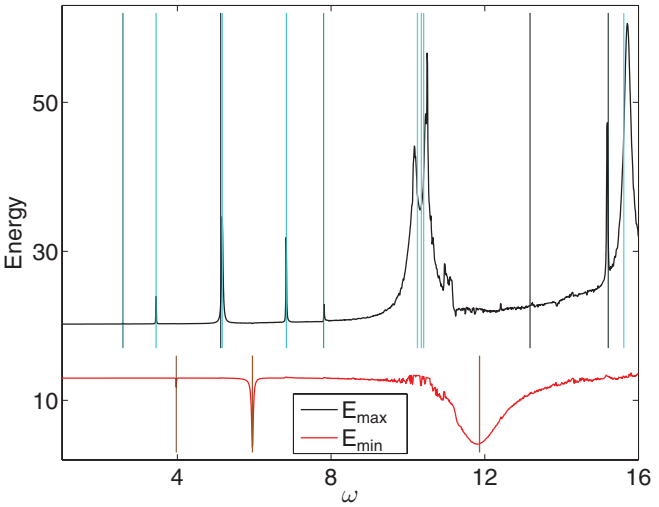

FIG. 6. (Color online) Analog of Fig. 2 for the breathing driving law. Numerical values can be taken from Table II. The parameters are the same as in Fig. 1.

lowest excited states are, however, very similar to the ones in Fig. 1 and consequently the resonances in Fig. 6 (compare also Table II) resemble the ones in Fig. 2. In Fig. 6 more resonances can be resolved due to a sufficiently small interaction time τ_{int}. This observation can be understood as follows: While for the axis-ratio-preserving driving law the transition matrix D_l^{nm} [Eq. (23)] is identical to zero due to $\dot{r}(t) = 0$, this is not the case for the breathing driving law. The additionally resolved resonances for the breathing law thus correspond to Landau-Zener transitions with $\dot{r}(t)$ being the Landau-Zener velocity [32]. This role of D_l^{nm} triggering Landau-Zener transitions will be even more pronounced for the next driving law that is presented.

The so-called volume-preserving driving law is just the opposite of the axis-ratio-preserving driving law. It keeps the volume $V(t)$ of the billiard fixed while varying the ratio of the semiaxes $r(t)$. Thus $b(t)$ depends on $a(t)$ [Eq. (42)] as

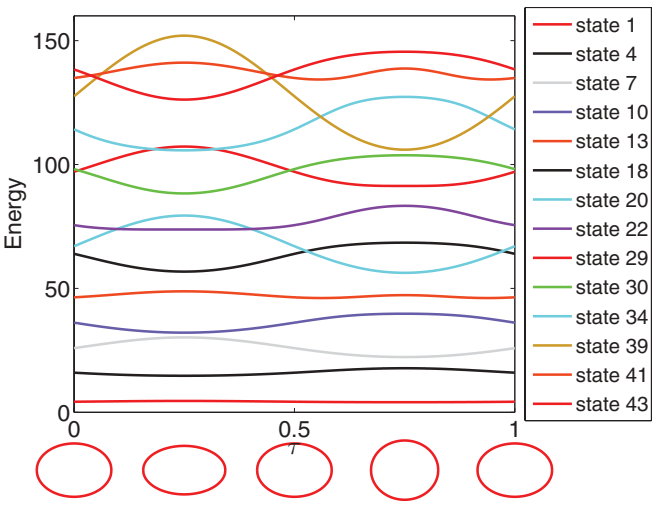

FIG. 7. (Color online) Energy eigenvalues $E_n(\tau)$ of eigenstates $|n;r(\tau)\rangle$ with even η- and ξ-parity eigenvalues for the volume-preserving driving law. The parameters are the same as in Fig. 1.

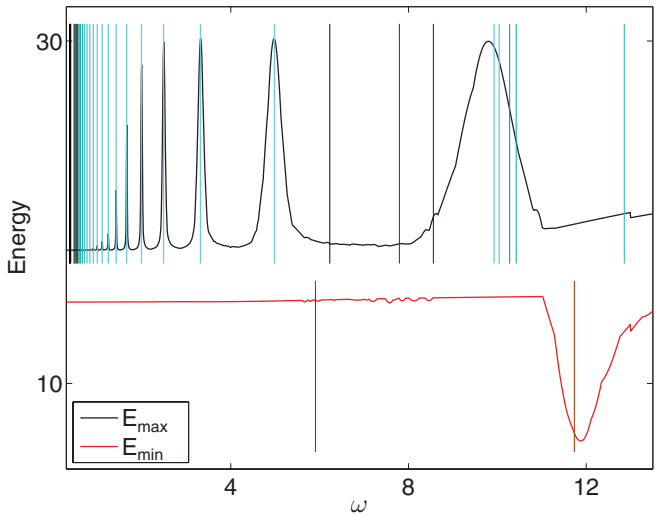

FIG. 8. (Color online) Analog of Fig. 2 for the volume-preserving driving law. Numerical values can be taken from Table III. The parameters are the same as in Fig. 1.

$b(t) = a_0 b_0 / a(t)$. Figure 7 shows the corresponding energy eigenvalues. We see that the fourth and seventh energy eigenvalues get close upon driving such that we expect that the transition matrix D_l^{nm} [Eq. (23)] couples these states strongly. We point out that we can arbitrarily control how close these eigenvalues get upon driving by choosing $r(t)$ appropriately. As D_l^{nm} [Eq. (23)] depends on ω only through the phase factor $e^{-(2\pi i/\omega)\Delta\nu_{mn}(\tau)}$, we expect it to be slowly varying with ω, thus setting an upper bound on the interaction time (35) of resonant population transitions between the fourth and seventh energy eigenstates even for small ω and corresponding large photon process orders l.

This expectation is fully confirmed by Fig. 8. All resolved resonances with $\omega < 5.5$ correspond exclusively to transitions between the fourth and seventh energy eigenstates. As U [Eq. (4)] gets close to identity for small driving frequencies ω, the induced resonance shift is negligible. One might wonder

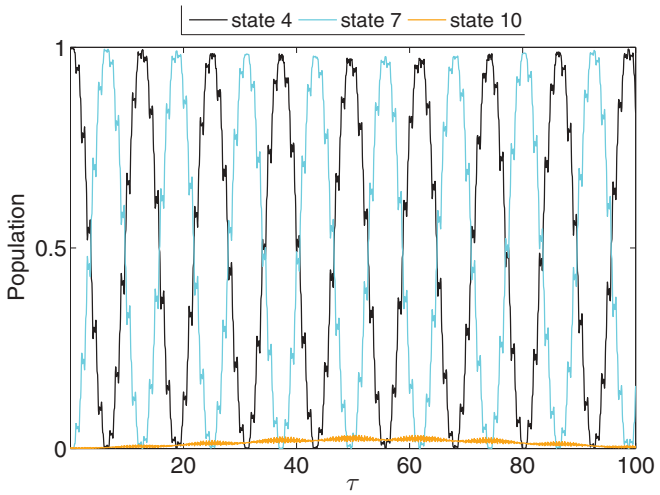

FIG. 9. (Color online) Population dynamics $p_n(\tau)$ for the volume-preserving driving law at $\omega = 3.32$. The parameters are the same as in Fig. 1.

why most of the resonances at small driving frequencies have numerically not been fully resolved even though their interaction time is short enough. In review of Eq. (32), we understand that a detuning in the driving frequency is also multiplied by the photon process order l. Thus one has to adjust the driving frequency very carefully to resolve a multiple-photon resonance. Note that Fig. 8 consists of 2500 data points, each requiring a full simulation of the quantum dynamics, yielding a total numerical effort of about 25 two-day runs on a computer cluster with 100 cores and 2.4 GHz each. We assume that using an even finer frequency grid in Fig. 8 would allow one to resolve even more of the predicted resonances.

Finally, population analyses close to the resonance frequencies confirm the Rabi-like behavior of the population dynamics as predicted by Eq. (41). This can be especially well illustrated for resonances with small interaction times. As an example, Fig. 9 shows almost perfect Rabi-like population dynamics of the fourth and seventh energy eigenstates in the nearly resonant case of a three-photon process at $\omega = 3.32$. A comparison of the observed beating periods with the corresponding interaction times τ_{int} in Table III gives, even quantitatively, very good agreement, as predicted by Eq. (40).

TABLE III. Analog to Table I, but for the volume-preserving driving law.

$\omega_{\text{res}}^{n4,l}$	τ_{int}	τ_{low}	State n	Order l
0.3682	1985	0.0367	7	3
0.3823	1889	0.0381	7	2
0.3976	1975	0.0397	7	4
0.4733	1176	0.0472	7	2
0.4970	842	0.0496	7	3
0.5232	741	0.0522	7	4
0.5522	712	0.0551	7	1
0.5847	525	0.0583	7	2
0.6213	303	0.0620	7	3
0.6627	185	0.0661	7	1
0.7100	124	0.0708	7	4
0.7647	88.6	0.0763	7	2
0.8284	63.7	0.0826	7	3
0.9037	45.0	0.0902	7	2
0.9941	31.3	0.0992	7	4
1.105	22.0	0.110	7	2
1.243	15.7	0.124	7	3
1.420	11.5	0.142	7	4
1.657	8.51	0.165	7	1
1.989	6.42	0.199	7	2
2.487	4.95	0.248	7	3
3.317	3.94	0.332	7	1
4.982	3.31	0.500	7	4
5.905	411	0.271	1	2
6.228	1134	0.555	13	3
7.795	691	0.691	13	2
8.559	875	1.98	20	4
9.926	28.9	1.01	10	2
10.04	2.97	1.02	7	3
10.28	347	2.33	20	4
10.42	218	0.912	13	1
11.74	5.06	0.538	1	2
12.86	136	2.83	20	3

We point out that as we can tune the strength of the transition matrix D_l^{nm} by choosing how close the energy eigenvalues get upon driving, we can also tune the interaction time τ_{int} in the regime of weak driving where it is mainly determined by D_l^{nm}. Hence we can in principle also control the beating period of the present effective two-level Rabi system.

IV. SUMMARY

A time-dependent perturbative approach for elliptical quantum billiards with oscillating boundaries has been developed. As our major results we have obtained a Fermi golden rule predicting the driving frequencies yielding resonant population transfer between instantaneous eigenstates as observed in Ref. [23] and a criterion allowing one to decide which of these resonances are observable in a corresponding experiment of certain duration. Extensive numerical simulations have been performed for three different driving laws, which are in excellent agreement with our predictions. Particularly for the volume-preserving driving law, due to the change of the billiard geometry upon driving, Landau-Zener transitions have been observed to take place. Depending only weakly on the driving frequency, these transitions allow for resonant population transfer also for very weak driving. We have shown that the billiard dynamics can be reduced in this regime to an effective two-level system with in principle arbitrarily tunable oscillation period. Further interesting phenomena beyond the scope of our perturbative description can be expected in the numerically challenging regime of strong driving.

ACKNOWLEDGMENT

B.L. thanks the Landesexzellenzinitiative Hamburg "Frontiers in Quantum Photon Science," which is funded by the Joachim Herz Stiftung, for financial support.

APPENDIX: MATRIX ELEMENTS

We introduce the matrices

$$\hat{f}^1 = \sum_{n,m,n',m'} |\Phi_{n,m}\rangle \delta_{m,m'} f^1_{nmn'} \langle \Phi_{n',m'}|, \tag{A1}$$

$$\hat{f}^2 = \sum_{n,m,n',m'} |\Phi_{n,m}\rangle \delta_{m,m'} f^2_{nmn'} \langle \Phi_{n',m'}|, \tag{A2}$$

$$\hat{f}^3 = \sum_{n,m,n',m'} |\Phi_{n,m}\rangle \delta_{(m-2),m'} f^3_{nmn'} \langle \Phi_{n',m'}|, \tag{A3}$$

$$\hat{f}^4 = \sum_{n,m,n',m'} |\Phi_{n,m}\rangle \delta_{(m-2),m'} f^4_{nmn'} \langle \Phi_{n',m'}|, \tag{A4}$$

$$\hat{f}^5 = \sum_{n,m,n',m'} |\Phi_{n,m}\rangle \delta_{(m+2),m'} f^5_{nmn'} \langle \Phi_{n',m'}|, \tag{A5}$$

$$\hat{f}^6 = \sum_{n,m,n',m'} |\Phi_{n,m}\rangle \delta_{(m+2),m'} f^6_{nmn'} \langle \Phi_{n',m'}|, \tag{A6}$$

with matrix elements

$$f^1_{nmn'} = \frac{-k^2_{m,n}}{4} \delta_{n,n'}, \tag{A7}$$

$$f^2_{nmn'} = \frac{1}{2J_{m+1}(k_{m,n})J_{m+1}(k_{m,n'})} \times \int_0^1 J_m(k_{m,n}r) J_m(k_{m,n'}r) r^3 dr, \tag{A8}$$

$$f^3_{nmn'} = \frac{k^2_{m-2,n'}}{4J_{m+1}(k_{m,n})J_{m-1}(k_{m-2,n'})} \times \int_0^1 J_m(k_{m,n}r) J_m(k_{m-2,n'}r) r\, dr, \tag{A9}$$

$$f^4_{nmn'} = \frac{1}{4J_{m+1}(k_{m,n})J_{m-1}(k_{m-2,n'})} \times \int_0^1 J_m(k_{m,n}r) J_{m-2}(k_{m-2,n'}r) r^3 dr, \tag{A10}$$

$$f^5_{nmn'} = \frac{k^2_{m+2,n'}}{4J_{m+1}(k_{m,n})J_{m+3}(k_{m+2,n'})} \times \int_0^1 J_m(k_{m,n}r) J_m(k_{m+2,n'}r) r\, dr, \tag{A11}$$

$$f^6_{nmn'} = \frac{1}{4J_{m+1}(k_{m,n})J_{m+3}(k_{m+2,n'})} \times \int_0^1 J_m(k_{m,n}r) J_{m+2}(k_{m+2,n'}r) r^3 dr, \tag{A12}$$

where J_m is again the cylindrical Bessel function of order m and $k_{m,n}$ is its nth root. We have a convenient form of representing H_M [Eq. (9)], $M(r)$ [Eq. (12)], and $H_F(\tau)$ [Eq. (10)] in the eigenbasis $\{|\Phi_{n,m}\rangle\}_{n,m}$ [Eq. (8)] of the static circular billiard:

$$H_M = g_1(\tau)\hat{f}^1 + g_3(\tau)(\hat{f}^3 + \hat{f}^5), \tag{A13}$$

$$M(r) = -\left(r + \frac{1}{r}\right)\hat{f}^1 - \left(r - \frac{1}{r}\right)(\hat{f}^3 + \hat{f}^5), \tag{A14}$$

$$H_F(\tau) = g_2(\tau)\hat{f}^2 + g_4(\tau)(\hat{f}^4 + \hat{f}^6). \tag{A15}$$

Diagonalizing $M(r)$ yields the instantaneous eigenstates $|n;r\rangle$ and their eigenvalues $q_n(r)$. One could in principle calculate the energy eigenvalues $E_n(\tau) = \frac{\hbar^2}{\mu V(\tau)} q_n[r(\tau)]$ from the $q_n(r)$, but it turns out that diagonalizing H_M directly increases the numerical precision of the energy eigenvalues. Note that the time-dependent factors $g_i(\tau)$ as well as the matrix elements $f^i_{nmn'}$ are the same as in Ref. [23]. However, the matrix elements $f^i_{nmn'}$ have been reduced to a much simpler form, using orthonormality relations of the Bessel functions

$$g_1(\tau) = -\frac{\hbar^2}{\mu}\left(\frac{1}{a(\tau)^2} + \frac{1}{b(\tau)^2}\right), \tag{A16}$$

$$g_2(\tau) = \mu[a(\tau)\ddot{a}(\tau) + b(\tau)\ddot{b}(\tau)], \tag{A17}$$

$$g_3(\tau) = -\frac{\hbar^2}{\mu}\left(\frac{1}{a(\tau)^2} - \frac{1}{b(\tau)^2}\right), \tag{A18}$$

$$g_4(\tau) = \mu[a(\tau)\ddot{a}(\tau) - b(\tau)\ddot{b}(\tau)]. \tag{A19}$$

Further note that the sign of $g_3(\tau)$ is inverted in comparison with Ref. [23]. We can now calculate the transition matrix elements D_l^{nm} [Eq. (23)] and F_l^{nm} [Eq. (22)]:

$$D_l^{nm} = v^{nm}_{1,l} + v^{nm}_{2,l}, \tag{A20}$$

$$F_l^{nm} = v^{nm}_{3,l} + v^{nm}_{4,l}, \tag{A21}$$

$$v_{1,l}^{nm} = -i \int_0^1 d\tau\, e^{2\pi i l\tau} e^{-(2\pi i/\omega)\Delta\nu_{mn}(\tau)} \left(r - \frac{1}{r}\right) \times \frac{\dot{r}}{r} \frac{\langle n;r|\hat{f}^1|m;r\rangle}{q_n(r) - q_m(r)}, \tag{A22}$$

$$v_{2,l}^{nm} = -i \int_0^1 d\tau\, e^{2\pi i l\tau} e^{-(2\pi i/\omega)\Delta\nu_{mn}(\tau)} \left(r + \frac{1}{r}\right) \times \frac{\dot{r}}{r} \frac{\langle n;r|\hat{f}^3 + \hat{f}^5|m;r\rangle}{q_n(r) - q_m(r)}, \tag{A23}$$

$$v_{3,l}^{nm} = \frac{1}{2\pi\hbar} \int_0^1 d\tau\, e^{2\pi i l\tau} e^{-(2\pi i/\omega)\Delta\nu_{mn}(\tau)} g_2(\tau)\, \langle n;r|\hat{f}^2|m;r\rangle, \tag{A24}$$

$$v_{4,l}^{nm} = \frac{1}{2\pi\hbar} \int_0^1 d\tau\, e^{2\pi i l\tau} e^{-(2\pi i/\omega)\Delta\nu_{mn}(\tau)} g_4(\tau) \times \langle n;r|\hat{f}^4 + \hat{f}^6|m;r\rangle. \tag{A25}$$

After calculating these quantities and diagonalizing $M(r)$ and H_M, it is straightforward to reproduce the theoretical predictions contained in this work.

[1] A. Loskutov, A. Ryabov, and E. D. Leonel, Physica A **389**, 5408 (2010).
[2] D. R. da Costa, C. P. Dettmann, and E. D. Leonel, Phys. Rev. E **83**, 066211 (2011).
[3] E. D. Leonel and C. P. Dettmann, Phys. Lett. A **376**, 1669 (2012).
[4] D. U. Matrasulov, U. R. Salomov, G. M. Milibaeva, and N. E. Iskandarov, Physica D **240**, 470 (2011).
[5] F. Lenz, F. K. Diakonos, and P. Schmelcher, Phys. Rev. Lett. **100**, 014103 (2008).
[6] A. Loskutov, A. B. Ryabov, and L. G. Akinshin, J. Phys. A **33**, 7973 (2000).
[7] D. F. M. Oliveira, J. Vollmer, and E. D. Leonel, Physica D **240**, 389 (2011).
[8] E. D. Leonel and L. A. Bunimovich, Phys. Rev. E **82**, 016202 (2010).
[9] E. D. Leonel and L. A. Bunimovich, Phys. Rev. Lett. **104**, 224101 (2010).
[10] F. Lenz, C. Petri, F. K. Diakonos, and P. Schmelcher, Phys. Rev. E **82**, 016206 (2010).
[11] K. Shah, D. Turaev, and V. Rom-Kedar, Phys. Rev. E **81**, 056205 (2010).
[12] B. Liebchen, R. Büchner, C. Petri, F. K. Diakonos, F. Lenz, and P. Schmelcher, New J. Phys. **13**, 093039 (2011).
[13] A. Y. Loskutov, A. B. Ryabov, and L. G. Akinshin, J. Exp. Theor. Phys. **89**, 966 (1999).
[14] L. E. Reichl, *The Transition to Chaos* (Springer, New York, 1992).
[15] H.-J. Stöckmann, *Quantum Chaos: An Introduction* (Cambridge University Press, Cambridge, 1999).
[16] E. Fermi, Phys. Rev. **75**, 1169 (1949).
[17] A. J. Lichtenberg and M. A. Liebermann, *Regular and Chaotic Dynamics* (Springer, New York, 1992).
[18] F. Lenz, Ph.D. thesis, Universität Heidelberg, 2009.
[19] T. Hogg and B. A. Huberman, Phys. Rev. Lett. **48**, 711 (1982).
[20] P. Seba, Phys. Rev. A **41**, 2306 (1990).
[21] J. F. Willemsen, Phys. Rev. E **50**, 3116 (1994).
[22] K. Nakamura, S. K. Avazbaev, Z. A. Sobirov, D. U. Matrasulov, and T. Monnai, Phys. Rev. E **83**, 041133 (2011).
[23] F. Lenz, B. Liebchen, F. K. Diakonos, and P. Schmelcher, New J. Phys. **13**, 103019 (2011).
[24] D. Cohen and D. A. Wisniacki, Phys. Rev. E **67**, 026206 (2003).
[25] R. L. Liboff and M. A. Porter, Chaos **10**, 366 (2000).
[26] J. Orear and E. Fermi, *Nuclear Physics: A Course Given by Enrico Fermi at the University of Chicago* (University of Chicago Press, Chicago, 1950).
[27] R. W. Robinett, Am. J. Phys. **64**, 440 (1996).
[28] R. W. Robinett, Eur. J. Phys. **24**, 231 (2003).
[29] M. Born and V. Fock, Z. Phys. A **51**, 165 (1928).
[30] W. Vogel and D. G. Welsch, *Quantum Optics* (Wiley-VCH, Weinheim, 2006).
[31] L. Mandel and E. Wolf, *Optical Coherence and Quantum Optics* (Cambridge University Press, Cambridge, 1995).
[32] C. Zener, Proc. R. Soc. London Ser. A **137**, 696 (1932).